ABA-activated nanomolar Ca^{2+}-CPK signalling controls root cap cycle plasticity and stress adaptation

Kun-Hsiang Liu (khliu@molbio.mgh.harvard.edu)
North West Agriculture and Forestry University
Ziwei Lin
North West Agriculture and Forestry University
ying Guo
North West Agriculture and Forestry University
Ruiyuan Zhang
North West Agriculture and Forestry University
Yiming Li
North West Agriculture and Forestry University
Yue Wu
Massachusetts General Hospital
Jen Sheen
Massachusetts General Hospital https://orcid.org/0000-0001-8970-9267

Article

Keywords:

Posted Date: February 14th, 2024

DOI: https://doi.org/10.21203/rs.3.rs-3929094/v1

Additional Declarations: There is **NO** Competing Interest.

Abstract

Abscisic acid (ABA) regulates plant stress adaptation, growth, and reproduction. Despite extensive ABA-Ca^{2+} signaling links, imaging ABA-induced Ca^{2+} concentration increase was challenging, except in guard cells. Here, we visualize ABA-triggered [Ca^{2+}] dynamics in diverse organs and cell types using a genetically-encoded Ca^{2+} ratiometric sensor (CRS) with nanomolar affinity and large dynamic range. Subcellular-targeted CRS reveals time-resolved and unique spatiotemporal Ca^{2+} signatures from the initial plasma-membrane nanodomain, cytosol, to nuclear oscillation. Via receptors and sucrose-non-fermenting1-related protein kinases (SNRK2.2,2.3,2.6), ABA activates nanomolar Ca^{2+} waves and Ca^{2+}-sensor protein kinase (CPK10,30,32) signalling in the root cap cycle from stem cells to cell detachment. Surprisingly, unlike the prevailing NaCl-stimulated micromolar Ca^{2+} spike, salt stress induces a nanomolar Ca^{2+} wave through ABA signaling, repressing key transcription factors dictating cell fate and enzymes crucial to root cap maturation and slough. Our findings uncover ultrasensitive ABA-Ca^{2+}-CPK signalling in modulating root cap cycle plasticity in adaptation to adverse environments.

Introduction

ABA is a versatile and central plant hormone that regulates broad developmental processes throughout the plant lifecycle from embryogenesis, seed dormancy and germination, organ size, mass and architecture, and fertility, to integrative nutrient, metabolic, and hormone signalling networks[1–4]. In response to diverse stress environmental conditions, local and systemic synthesis and transport contribute to elevated ABA in various organs and cell types to enhance plant adaptation and protection to abiotic challenges[2–7]. ABA is perceived by its binding to many functionally redundant/overlapping receptors, PYRABACTIN RESISTANCE1 (PYR1)/PYR1-LIKE (PYL)/REGULATORY COMPONENTS OF ABA RECEPTORS (RCAR) [2]. ABA-bound RCAR/PYR1/PYL complexes with and inhibits the function of clade A Protein Phosphatase 2Cs (PP2Cs). In the absence of ABA, the phosphatase activity of PP2Cs inhibits the kinase activity of SnRK2.2/2.3/2.6, which positively regulates the ABA signalling network[2,3].

As a universal cellular messenger, Ca^{2+} mediates diverse signalling events in multiple subcellular compartments of all organisms[8,9]. Temporal patterns in the dynamics of [Ca^{2+}], so-called Ca^{2+} signatures, may appear as rapid spikes, transient or sustained waves, or oscillating peaks in [Ca^{2+}]. In the cytosol and organelles, such Ca^{2+} signatures are often attributed to specific signalling events in plant development and response to environmental cues[7–10]. Extensive research supports that Ca^{2+} signalling plays a central role in ABA responses, especially in guard cells[11–14]. For example, multiple Ca^{2+}-sensor protein kinases (CPK3/6/21/23) perceiving and relaying endogenous cytosolic $[Ca^{2+}]_{cyt}$ oscillations have been shown to phosphorylate and activate S-type anion channels, SLAC1 and SLAH3, to mediate ABA-induced stomata closure[11–18]. CPK4/11/10/30/32 are implicated in activating gene expression through phosphorylation and activation of ABA-responsive transcription factors (ABFs)[15,19–21]. Moreover,

CPK3/4/6/11 modulates ABA-induced phosphorylation and degradation of guanine nucleotide exchange factor RopGEF1 to facilitate ABA signalling in root hair development and cotyledon growth[22].

Despite molecular, cellular, biochemical, modelling, and genetic evidence supporting intimate ABA-Ca^{2+} signalling connections in leaf, root, and guard cells[11–22], direct imaging of ABA-stimulated cytosolic $[Ca^{2+}]_{cyt}$ oscillations was only feasible in guard cells over the past two decades[23]. It has been a long-standing mystery that $[Ca^{2+}]$ increase by ABA at single-cell resolution has never been visualized and quantified in other organs and cell types even with the intensity-based Ca^{2+} sensor R-GECO1 exhibiting a significantly increased sensitivity over the Förster Resonance Energy Transfer (FRET)-based Ca^{2+} reporter Yellow Cameleon NES-YC3.6 and YC-nano50[23–26].

Genetically-encoded Ca^{2+} indicators (GECIs) are indispensable tools for visualizing and quantifying Ca^{2+} signatures implicated in activating and specifying a broad spectrum of physiological and signalling functions in plant and animal cells. The GECIs aequorin, YC3.6, R-GECO1, and GCaMPs have been used to detect changes in local and systemic $[Ca^{2+}]$ induced by a variety of stimuli[9,10,23–30]. Aequorin is a bioluminescence-based Ca^{2+} indicator (*in vitro* K_d of 7.2–13 μM for Ca^{2+}) after reconstitution of the holoenzyme with the exogenously applied prosthetic group coelenterazine, and has been widely employed at the level of cell population or entire plants[9,10,30].

To enhance the spatiotemporal resolution and sensitivity of Ca^{2+} signalling at the single-cell level, fluorescent protein-based GECIs bind to Ca^{2+} with nanomolar K_d and are more sensitive to lower intracellular $[Ca^{2+}]$. Although R-GECO1 (K_d of 482 nM) and YC3.6 (K_d of 250 nM) can detect nanomolar levels of $[Ca^{2+}]$, only the ultrasensitive GCaMP6s, exhibiting a high affinity with a K_d of 144 nM for Ca^{2+} and a large dynamic range, could detect clear nitrate-induced Ca^{2+} signatures in plant leaf and root cells[10,27–30]. To directly visualize and quantify the elusive Ca^{2+} signatures induced by ABA in various plant organs and cell types, we needed new GECI tools, which will enable exploring novel ABA-Ca^{2+} signalling mechanisms and discovering new ABA functions in plant development and stress adaptation.

Results

Visualizing and quantifying ABA-triggered $[Ca^{2+}]$ dynamics at single-cell resolution

We postulated that an ultrasensitive GECI might reliably detect ABA-induced Ca^{2+} signals in various plant cell types. To support this hypothesis, we performed time-lapse recordings of ABA responses in the roots of transgenic GCaMP6s plants[10,27]. ABA triggered rapid and specific Ca^{2+} waves with dual peaks at 100–200 s in the root tip never previously observed, which were distinct from ABA-activated Ca^{2+} oscillations in guard cells[23,25,26] (Extended Data Fig. 1). To simplify and improve the quantification of GCaMP6s and

maintain its Ca^{2+} sensitivity and high dynamic range, we created a synthetic gene that expressed a single protein with two fluorescent proteins—the green fluorescent GCaMP6s and red fluorescent dTomato—fused by a short SSGS linker (Fig. 1a,b). In this simple Ca^{2+} ratiometric sensor (CRS), the C-terminal dTomato served as a stable internal control insensitive to Ca^{2+} and did not interfere with the Ca^{2+} binding of the N-terminal GCaMP6s (Fig. 1c). While the Ca^{2+}-induced green fluorescence of CRS was inhibited by EGTA chelation of Ca^{2+}, the red fluorescence of CRS was unaffected (Fig. 1c). Thus, the ratio of Ca^{2+}-sensitive green fluorescence to Ca^{2+}-insensitive red fluorescence of CRS with excitation at 488 nm and 554 nm, respectively, indicates the relative Ca^{2+} signal changes independent of protein expression levels. The K_d of CRS for Ca^{2+} was 165 nM by *in vitro* binding assays and was comparable to that of GCaMP6s (Fig. 1d)[27,30]. As a positive control, we first measured $[Ca^{2+}]$ dynamics after nitrate stimulation in the mesophyll protoplasts transiently expressing CRS. The ratio of green to red fluorescence reported a similar dynamic Ca^{2+} profile as previously recorded using GCaMP6s (Fig. 1e)[10]. Remarkably, we also detected reliable ABA-induced $[Ca^{2+}]$ dynamics with a distinct cytosolic pattern and lower amplitude in the transfected mesophyll protoplasts, but not in the mock control without ABA (Fig. 1f,g)[10].

To enable analyses of ABA-induced Ca^{2+} responses in different plant organs and cell types, we generated CRS transgenic plants. Because ABA-induced Ca^{2+} oscillations were previously observed in guard cells, we first validated the use of CRS in transgenic plants by analysing ABA-induced Ca^{2+} response in guard cells. Ca^{2+} oscillations in the cytosol of guard cells were observed only after ABA stimulation (Fig. 2a and Extended Data Fig. 2). We then monitored specific ABA-triggered Ca^{2+} responses in different organs, tissues, and cell types, not previously feasible. After ABA treatment, the stimulated mesophyll cells initiated a slower Ca^{2+} wave featuring a different shape and kinetic compared with the faster and more sustained Ca^{2+} wave in the root tip or root differentiation zone, or the rapid and sharper Ca^{2+} wave in the lateral root primordium (Fig. 2b-e). CRS-based live imaging in plants revealed for the first time that ABA could trigger diverse Ca^{2+} signatures distinct from Ca^{2+} oscillations in guard cells and might activate different cellular Ca^{2+} sensors to relay ABA signalling responses in various organs and cell types, as implicated by ABA reporters and next-generation ABACUS biosensors[1–7,11–23,31,32].

Dynamic spatiotemporal patterns of ABA-triggered Ca^{2+} signatures

Nitrate and ABA appeared to activate different subcellular patterns of $[Ca^{2+}]$ changes and dynamics in mesophyll protoplasts (Fig. 1e-g)[10]. Unlike GCaMP6s detecting nanomolar $[Ca^{2+}]$ changes in both the cytosol and the nucleus[10], CRS was restricted in detecting cytosolic $[Ca^{2+}]_{cyt}$. To overcome the subcellular limit of CRS, we created new versions of CRS localized at the plasma membrane or specific organelles to further characterize the high spatiotemporal resolution of Ca^{2+} signatures in different subcellular compartments (Fig. 3a). Importantly, transgenic plants expressing CRS fusion proteins showed no obvious growth defect phenotype (Extended Data Fig. 3). We analyzed ABA-triggered Ca^{2+} signatures in

transgenic plants stably expressing the CRS fusion protein variants targeted to the plasma membrane (CRS-PM), cytosol (CRS), or nucleus (CRS-NLS). As the root tip exhibited prominent ABA-responsive reporter gene expression[31] and Ca^{2+} dynamics (Extended Data Fig. 1 and Fig. 2c), we monitored time-resolved ABA-triggered [Ca^{2+}] change patterns in subcellular compartments in the uniform-shaped epidermal cells in the root meristematic zone (Fig. 2c, Fig. 3b-f and Extended Data Fig. 4, 5). When treated with ABA, cells expressing CRS-PM displayed the most rapid elevation of Ca^{2+} signals (< 50 s), which appeared to represent the first phase of two-phase cytosolic Ca^{2+} increases in timing and amplitude (Extended Data Fig. 1). The second phase of the elevated cytosolic Ca^{2+} signal was sustained for more than 5 min when significant decline occurred near the plasma membrane after 2 min. Unexpectedly, slower (approximately 100 s) but striking Ca^{2+} oscillation was observed with CRS-NLS (Fig. 3b-d and Extended Data Figs. 4 and 5). Imaging cytosolic [Ca^{2+}] changes in single cells expressing CRS variants suggests that the initial Ca^{2+} signal increase due to ABA treatment might be originated at the discrete nanodomains of the plasma membrane, and then spread throughout the plasma membrane before migrating to the cytosol and into the nucleus (Fig. 1f and Fig. 3b-d and Extended Data Figs. 4 and 5). The findings are consistent with the detection of ABA receptors and PP2C/ABI1-CPK21 signalling complexes on the plasma membrane nanodomains[33–35]

To directly visualize high spatiotemporal ABA-Ca^{2+} signalling processes at the single-cell resolution, we performed time-lapse imaging analysis along the plasma membrane of single CRS-expressing mesophyll cells exhibiting slower ABA-activated [Ca^{2+}] dynamics (Fig. 1f, g and Fig. 2b). We found that ABA-triggered Ca^{2+} signal elevations could start from discrete sites and were not evenly distributed along the plasma membrane before migrating into the cytosol (Extended Data Fig. 6a). In the root tip with faster ABA-Ca^{2+} signalling (Extended Data Fig. 1 and Fig. 2c), the CRS seedlings were treated with extracellular Ca^{2+} chelator, EGTA or BAPTA, or a plasma membrane Ca^{2+} channels blocker, $GdCl_3$, the ABA-induced cytosolic Ca^{2+} waves were abolished (Extended Data Fig. 6b). To further demonstrate the ABA-triggered Ca^{2+} signal was first initiated near the plasma membrane and distinct from the internal nitrate-Ca^{2+} signalling in GCaMP6s expressing mesophyll protoplasts[10], we generated a transgenic line harbouring dual CRS-PM and CRS-NLS sensors (CRS-PM/CRS-NLS). When CRS-PM/CRS-NLS seedlings were treated with ABA, Ca^{2+} signals first appeared near the plasma membrane at 10–20 s and then in the nucleus at 50 s in the single epidermal cells of the primary root meristem (Fig. 3e). We further conducted a higher-resolution kymography analysis of CRS-PM in response to ABA by dividing the perimeter of a single root epidermal cell into 440 adjacent regions (Fig. 3f). Combining live imaging analyses in single leaf and root cells with CRS variants provided strong evidence that elevated Ca^{2+} signals originated along the plasma membrane by ABA was not homogeneously distributed. CRS enabled the ultrasensitive detection of distinct extracellular and intracellular Ca^{2+} sources and dynamics in ABA and nitrate signalling, respectively[10].

Calibration of CRS for quantifying intracellular [Ca^{2+}]

To quantify the precise in vivo nanomolar cytosolic $[Ca^{2+}]_{cyt}$ in response to ABA, we recorded $[Ca^{2+}]$ changes in the root tip of CRS transgenic plant in response to ABA using two references generated by extracellular ATP (eATP)-activated micromolar increase in $[Ca^{2+}]$ and Ca^{2+} chelators to deplete free Ca^{2+} in the root tip cells (Fig. 4a)[24–26]. To calibrate and calculate the Ca^{2+} concentration of CRS in the root tip cells, we first treated CRS seedlings with eATP to saturate cellular Ca^{2+} and obtain the maximum fluorescence intensity and ratio. We then incubated the same plants in EGTA and BAPTA-AM to acquire the minimum fluorescence intensity and ratio. Since the *in vitro* K_d of CRS for Ca^{2+} is 165 nM, the maximum and minimum fluorescence intensity ratios were set at 330 nM and 0 nM, respectively, to calculate the intracellular $[Ca^{2+}]$ activated by ABA in the root tip (Fig. 4a,b). ABA increased $[Ca^{2+}]_{cyt}$ to ~ 164.3 nM in the root tip cells expressing CRS.

ABA-triggered nanomolar $[Ca^{2+}]$ wave via ABA receptors and SNRK2.2/2.3/2.6

Despite decades of intensive research[11–26], how ABA activates $[Ca^{2+}]$ increase remained unknown in most cell types except guard cells[14,23]. Arabidopsis PYR1 and PYL1/2/4/5/8 are functionally redundant ABA receptors that regulate ABA inhibition of primary root formation, while SNRK2.2/2.3/2.6 are key activators of ABA signalling[2,3,34,35]. To determine whether ABA-triggered $[Ca^{2+}]$ increase requires ABA receptors and SNRK2.2/2.3/2.6, we generated stable transgenic lines expressing CRS in the sextuple *pyrpyl112458* and triple *snrk2.2,2.3,2.6* mutants[34,35]. The ABA-induced $[Ca^{2+}]$ increase was eliminated in the *pyrpyl112458-CRS* and *snrk2.2,2.3,2.6-CRS* mutants, (Fig. 4c,d). To show that the abolished $[Ca^{2+}]$ increase was not due to CRS failure, we treated the same seedlings with eATP after recording the ABA responses. Striking $[Ca^{2+}]$ rise was induced by eATP in *pyrpyl112458*-CRS and *snrk2.2,2.3,2.6*-CRS, indicating that the ABA-triggered $[Ca^{2+}]$ increase is specifically regulated downstream of ABA receptors and SNRK2.2/2.3/2.6 (Fig. 4e,f).

The delayed root cap differentiation cycle by ABA-Ca-CPK signalling

CRS detected conspicuous ABA-triggered Ca^{2+} signalling in the root tip (Extended Data Fig. 1, Fig. 2c, and Fig. 4) where the root cap is located and plays essential functions in stem cell niche protection, gravitropism, thigmotropism, water/nutrient sensing and uptake, root system architecture, as well as protection from biotic and abiotic stress[36–40]. To explore ABA-Ca^{2+} signalling functions and regulatory mechanisms in the root cap, we examined the effect of ABA on the unique root cap cycle encompassing the differentiation programs of the columella and lateral root cap cells from stem cell regulation, differentiation, and maturation, to detachment (Fig. 5a) [36–40]. We first defined the periodicity of the root cap cycle by live imaging of the root cap morphology changes at 3-h intervals for 48 h starting with 5-day-old seedlings using an ECHO Revolve microscope (ECHO) (Fig. 5b). The average cycle period of root cap initiation and sloughing is approximately 30.4 ± 0.5 h (Fig. 5b). ABA treatment delayed the root cap cycle to approximately 34 ± 0.4 h. To further confirm the involvement of ABA in regulating the root cap

cycle, we examined ABA regulation in the sextuple ABA receptor *pyrpyl112458* mutant (Fig. 5b). The *pyrpyl112458* mutant was insensitive to ABA treatment in delaying root cap cycle. Since ABA triggered a maximum $[Ca^{2+}]_{cyt}$ of 164.3 nM in the root tip of the CRS seedlings (Fig. 4a), previous studies suggested that CPK10/30/32 with a higher Ca^{2+} sensitivity than other CPK subgroups may participate in ABA signalling[10,15,18–20,41]. To test if CPK10/30/32 may serve as the Ca^{2+} sensors to decode ABA-Ca^{2+} signalling in modulating the root cap cycle, we assessed the ABA response in the chemical-inducible triple *icpk* mutant (Fig. 5c)[10]. In the *icpk* seedling without 3MBiP

(1-isopropyl-3-(3-methylbenzyl)-1H-pyrazolo[3,4-d]pyrimidin-4-amine) induction[10], the average period of root cap cycle was similar to that in WT at approximately 31.5 ± 0.7 h. ABA treatment delayed the root cap cycle to 37.5 ± 0.7 h, but was reduced to approximately 34.3 ± 0.4 h in *icpk* (Fig. 5c).

To elucidate the molecular function of ABA in regulating the root cap cycle, we investigated the expression of key marker genes involved in regulating the differentiation processes. Transcription factor FEZ controls the columella stem cells and the epidermal/lateral root cap stem cells responsible for the initiation of the root cap. Transcription factor SOMBERO (SMB) represses FEZ to promote root cap differentiation, whereas BEARSKIN 2 (BRN2) is a central transcription factor for the maturation and detachment processes by activating target genes encoding enzymes involved in cell wall degradation, e.g., CELLULASE 5 (CEL5), PECTINESTERASE (PE11), and XYLOGLUCAN ENDOTRANSGLUCOSYLASE 5 (XTH5), and programmed cell death, including RIBONUCLEASE *3* (RNS3), and *METACASPASE* 9 (MC9) (Fig. 5a)[36–40]. RT-qPCR analysis was performed on RNA isolated from the root tip of WT and *pyrpyl112458* mutants without or with ABA. The results revealed that ABA activated a typical marker gene *KIN1*[14] but repressed *FEZ, SMB*, *BRN2*, *CEL5, XTH5, PE11, RNS3*,and *MC9* expression (Fig. 5d and Extended Data Fig. 7a). The ABA repression of these genes was abolished in the *pyrpyl112458* mutant (Fig. 5d, Extended Data Fig. 7a). Similarly, ABA repression of *SMB, BRN2, CLE5, PE11, RNS3*, and *MC9* was significantly reduced in the *icpk* mutant. The ABA repression of *FEZ*, *CEL5*, and *XTH5* required ABA receptors but was CPK10/30/32 independent (Fig. 5e, Extended Data Fig. 7b). These data further support the hypothesis that ABA-Ca^{2+}-CPK signalling is involved in regulating the root cap cycle by suppressing the expression of key genes in the developmental program of the entire root cap cycle.

Altering the root cap cycle plasticity by unique salt-ABA-Ca^{2+} signalling

Current knowledge supports that high salt stress triggers a transient and strong $[Ca^{2+}]$ increase and the classical salt-overly-sensitive (SOS) signalling pathway mediated by the Ca^{2+} sensor SOS3 (CBL4), the protein kinase SOS2 (CIPK24) and the Na^+/H^+ antiporter SOS1 in roots[28,42,43]. Little was known about salt stress effects on root cap cells. In CRS transgenic plants, we confirmed that 200 mM NaCl activated a sharp 50-s cytosolic Ca^{2+} spike in the root elongation zone (Fig. 6a)[28]. Unexpectedly, in contrast to the prevailing NaCl-activated micromolar $[Ca^{2+}]$ spike, salt stress activated sustained nanomolar $[Ca^{2+}]$ wave

in root cap cells (Fig. 6b) and significantly delayed the root cap cycle (Fig. 6c). This novel salt-stimulated [Ca^{2+}] increase was predominantly dependent on ABA signalling as it was significantly attenuated in the *pyrpyl112458*-CRS and *snrk2.2,2.3,2.6*-CRS mutants (Fig. 6b). Our result suggests the involvement of two salt signalling pathways, ABA-independent and ABA-dependent, and the later orchestrates the salt stress-induced changes in [Ca^{2+}] in the root cap. To assess the impact of salt stress on the regulation of the root cap cycle, we established a long-term observation method to investigate salt stress-induced phenotypes. Five-day-old seedlings were treated with 50 mM NaCl and the differentiation, maturation, and detachment of the root cap were monitored under a microscope every 3 h for 60 h. The average period of the root cap cycle from initiation to shedding was delayed from 31.4 ± 0.7 h (in mock treatment) to approximately 41.1 ± 0.6 h with NaCl treatment (Fig. 6c). The delayed root cap cycle showed insensitivity in the *pyrpyl112458* and *snrk2.2,2.3,2.6* mutants with 50 mM NaCl treatment (Fig. 6c). Additionally, RT-qPCR analysis was performed with RNA isolated from the root tip of WT seedlings with or without 200 mM NaCl treatment. Salt stress activated the expression of *KIN1*, a salt-stress- and ABA-responsive gene[21], while repressed *FEZ, SMB*, *BRN2*, *PE11*, *RNS3*, *MC9*, *XTH5*, and *CEL5* expression (Fig. 6d, Extended Data Fig. 8) similar to the ABA repression (Fig. 5d,e and Extended Data Fig. 7). The data presented here connect salt stress to the previously unknown endogenous ABA and Ca^{2+} signalling in controlling the root cap cycle (Fig. 6e).

Discussion

Despite decades of research, the full physiological functions of ABA as a versatile plant hormone and its wide-ranging signalling mechanisms remain incompletely understood[1–7,11–23,31,32]. The molecular links of ABA-Ca^{2+} signalling were especially enigmatic in most plant organs and cell types[11–26]. The simple design and easy application and modification of CRS offer several advantages over other prevalent Ca^{2+} biosensors, e.g., aequorin, YC3.6, YCnano50, and R-GECO1[23–30], for new investigations of ABA-Ca^{2+} signalling in plants. CRS exhibits high sensitivity, large dynamic range, and fast response. The single-cell ratiometric imaging by the stable single fusion of GCaMP6s[10,27–30] and dTomato for dual fluorescence displays low phototoxicity and is suitable for tagged protein monitoring. CRS and its variants localized in different subcellular compartments and organelles represent ultrasensitive and versatile Ca^{2+} imaging tools enabling real-time quantitative and comparative detection of high spatiotemporal resolution without disturbing plant growth and development[25,29]. With CRS, we demonstrate that ABA triggers different and previously unknown cytosolic Ca^{2+} signatures in shoot and root cells distinct from the Ca^{2+} oscillation in guard cells[23]. Despite a high correlation between ABA and abiotic stress, ABA-induced cytosolic Ca^{2+} signals are strikingly slower but more sustained with lower amplitude compared with the rapid, strong, and very transient and sharp Ca^{2+} spikes characteristic of cold, salt, and osmotic stress responses[8,9,28,30]. Direct visualization and recording of distinct [Ca^{2+}] dynamics with CRS and its subcellular derivatives could be broadly applied in investigating physiological responses to other phytohormone, nutrient, chemical, physical, or peptide signals that may elicit exquisite and specific Ca^{2+} responses in localized subcellular compartments and nanodomains with previously unrecognized physiological roles in plants.

Chelating apoplast Ca^{2+} by EGTA and BAPTA blocked ABA-induced [Ca^{2+}] changes, suggesting the extracellular source of Ca^{2+} in root cells in response to ABA. Distinct patterns of ABA-activated [Ca^{2+}] dynamics, initiating from the plasma membrane, migrating to the cytoplasm, and triggering nuclear oscillation, further support this hypothesis. ABA-induced Ca^{2+} signalling appears to initiate at nanodomains of the plasma membrane in leaf mesophyll and root meristem epidermal cells consistent with the detection of ABA receptors and signalling components[33,35]. Rapid Ca^{2+} propagation around the plasma membrane may reflect positive feedback in Ca^{2+} signalling associated with recruiting more ABA receptor complexes[33,35] for amplified and sustained Ca^{2+} channel activation[14]. Future research may reveal whether specific nanodomains are enriched with Ca^{2+} channels and/or ABA signalling components and how [Ca^{2+}] dynamics are decoded and coordinated for cell-type and organelle- or subcellular-specific ABA responses.

FRET-based ABA indicators detect ABA accumulation in the root[32]. However, R-GECO1 Ca^{2+} indicator failed to detect ABA-triggered Ca^{2+} signals in roots[25,26]. Our results with CRS revealed that ABA triggered nanomolar [Ca^{2+}] increase up to approximately 164 nM calibrated in the root tip. Thus, only the ultrasensitive Ca^{2+} indicator such as GCaMP6s and CRS[10,27–30] can be used to circumvent the limitation of R-GECO1 and YC3.6[23–26]. Interestingly, we found that CPK10/30/32 are nanomolar Ca^{2+} sensors contributing to the signalling decoding specificity responsible for ABA and nitrate[10,41] responses in the root cap and perhaps also in other organs and cell types and in different subcellular compartments. In guard cells, CPK3/6/21/23, responsible for ABA signalling and relaying the unique cytosolic Ca^{2+} oscillation, appeared to require higher [Ca^{2+}] for full activation[15–18,41], The differential activation of different CPKs as natural plant Ca^{2+} sensors in different cell types in response to ABA may explain the detection of ABA-activated cytosolic Ca^{2+} oscillation by FRET-based YC2.1 and YC3.6 with lower dynamic range and Ca^{2+} affinity than GCaMP6s and CRS variants[15–18,41].

The application of CRS in *Arabidopsis* plants led to our discovery that ABA triggers [Ca^{2+}] dynamics in the root tip and delays the root cap cycle via PYR/PYL-SNRK2-CPK10/30/32 signalling. The findings suggest that ABA represses the root cap cycle as a stress adaptation and protection mechanism. As most research focused on ABA-activated genes[1–7,19–21], our study reveals the little-known functional significance of ABA-repressed genes encoding cell-fate regulating transcription factors and enzymes involved in cell-wall degradation and programmed cell death to modulate the root cap cycle plasticity. Further exploration of ABA-repressed genes may uncover novel ABA functions and regulatory mechanisms in plant development and reproduction[1–7,31,32].

In CRS transgenic plants, we confirmed that NaCl activated the prevailing [Ca^{2+}] spike in the root elongation zone. However, in contrast to the typical NaCl-activated micromolar [Ca^{2+}] spike, our study with CRS revealed that salt stress activates nanomolar [Ca^{2+}] wave via ABA leading to an increase in cytosolic [Ca^{2+}] specifically within root cap cells with concurrently delayed root cap cycle. It has been reported that it took 6 h in multiple root zones above the root cap to respond to shoot-derived ABA

stimulated by 100 mM NaCl treatment in *Arabidopsis* seedlings expressing nlsABACUS2 biosensors[32]. In the root cap, NaCl appeared to stimulate very rapid ABA-Ca^{2+} signalling within minutes which may represent a different source of local ABA. Moreover, salt and ABA signalling target and repress shared key transcription factors dictating cell fate and enzymes activating cell-wall degradation and cell death crucial to root cap maturation and slough. Unveiling the precise Ca^{2+} channel, transporter, or Ca^{2+}-permeable protein that facilitates ABA-mediated increases in cytosolic [Ca^{2+}] distinct from the canonical SOS signalling pathway will lead to new insight into plant salt stress signalling.

It is conceivable that Ca^{2+} signalling also interfaces with many other regulatory mechanisms in the root cap cycle. Exploiting the CRS transgenic line as a research tool holds the potential to address these inquiries through the investigation of Ca^{2+} signalling responses to diverse stimuli. Currently, the signalling mechanisms that converge and control the development of the root cap cycle are poorly understood. Future research will reveal the integrated regulatory network that modulates root cap development by other transcription factors, peptides, hormones, and environmental cues. For instance, how ABA and WOX5 transcription factor acting in the root quiescent centre synergistically block the differentiation of the root cap stem cells[31,44], and how ABA, auxin, and cytokinin signalling crosstalk in columella and lateral root cap cells[31,36,39,44,45]. Intriguingly, nitrate and ABA signalling interact and regulate the root cap cycle by initiating distinct subcellular Ca^{2+} waves but sharing ultrasensitive CPKs and NLP7 and SMB transcription factors[10,36–39]. It will also be important to determine the downstream signalling mechanisms that interconnect IDL1-HSL2 peptide-receptor kinase and ABA signalling with antagonistic functions in modulating the root cap cycle[40].

Methods

Plasmid Constructs and Transgenic Lines

To construct the CRS protein, the 1.3 kb GCaMP6s coding region was amplified by PCR from the *pHBT-GCaMP6s* plasmid[10] using primers GCaMP6s-F and GCaMP6s-R (Supplementary Table 1), and the 0.7 kb dTomato coding region was amplified by PCR from the *pHBT-tdTomato* plasmid[10] using primers dTomato-F and dTomato-R (Supplementary Table 1). The two amplified DNA fragments were fused with a GS linker (AGTTCCGGATCT) and subcloned into the BamHI and StuI sites of the *pHBT-tdTomato* plasmid using a Gibson Assembly® Master Mix kit (New England Biolabs). The plasmid *pUBQ10-CRS* was generated by replacing the HBT promoter with the *ubiquitin10* promoter using primers UBQ10-F and UBQ10-R (Supplementary Table 1).

To introduce the C-terminal targeting sequence (Supplementary Table 2) for nuclear or plasma membrane localization, oligonucleotides with the ATG start codon and appropriate restriction sites were designed and inserted into the *CRS* construct. Applying the *CRS* as a template, PCR was performed using the designed primers (Supplementary Table 1), and the amplified PCR products were cloned into the BamHI and StuI sites of the *CRS* vector using the Gibson Assembly method. The plasma membrane was

amplified from Arabidopsis genome DNA using the primers listed in Table S1 (Supplementary Table 1). The PCR fragments were cloned into the BamHI and StuI sites of the *CRS* plasmid using the Gibson Assembly method. The different *CRS* constructs were amplified and inserted into the binary vector *pGIIB-p35S-LIC-NOSt*[47], and the *Agrobacterium* (GV3101)-mediated floral-dip method was applied to generate transgenic plants harboring *CRS* constructs. The transgenic plants were selected after they had been sprayed with Basta® herbicide. To obtain *pyrpyl112458* and *snrk2.2,2.3,2.6* mutants expressing CRS, *pyrpyl112458* and *snrk2.2,2.3,2.6* were crossed to the CRS transgenic line. The homozygous *pyrpyl112458*-CRS and *snrk2.2,2.3,2.6*-CRS were characterized by genotyping.

Plant Materials and Growth Conditions

Arabidopsis ecotype Columbia (Col-0) was used as wild type (WT). To monitor ABA-triggered Ca^{2+} changes, 10–15 CRS, CRS-PM, and CRS-NLS transgenic seedlings were grown in each well of a six-well tissue culture plate (Corning) containing 1 mL of 1/2 Murashige & Skoog Basal Salt Mixture (MS) (Caisson) medium supplemented with 1 g/L MES and 1% sucrose at pH 5.8; the culture plate was maintained under 12 h light:12 h dark photoperiod conditions at 23°C for 7 days. To obtain nitrate-free protoplasts, the plants were grown as previously described[10]. To examine and compare the shoot development phenotypes in WT, CRS, CRS-NLS, CRS-PM, plants were grown in the soil (Pindstrup) under constant light (120 μmol m^{-2} s^{-1}mol) at 23°C for 21 days. Photos were taken using a digital camera (Canon DOS80D) and processed using Adobe photoshop (Adobe). To monitor root progression, one seedling was grown in each well of a 12-well tissue culture plate (Falcon) containing 0.5 mL of 1/2 MS medium, under constant light at 23°C for 5 days. For gene expression analyses performed using RT–qPCR, 10–15 seedlings were germinated in each well of a six-well tissue culture plate containing 1 mL of 1/2 MS medium supplemented with 1% sucrose, under constant light at 23°C for 5 days. To induce gene expression, WT or *pyrpyl112458* seedlings were induced with 1 mL of 1/2 MS medium containing 10 μM ABA or 0.1% ethanol (mock) for 4 h. WT and *icpk* seedlings were pretreated with 10 μM 3MBiP for 15 min and then treated for 4 h with either 10 μM ABA or or 0.1% ethanol (mock). For salt stress assay, seedlings were treated with 200 mM NaCl or H_2O (mock) in 1 mL of 1/2 MS medium for 2 h. From the root tip, one-third of the roots were cut and harvested for RNA extraction using a phenol-based extraction buffer[48] [38% phenol (Solarbio), 0.8 M guanidine thiocyanate (MilliporeSigma), 0.4 M ammonium thiocyanate (Shanghai yuanye Bio-Technology), 0.1 M sodium acetate, and 5% glycerol] at pH 5.2.

CRS-based Ca^{2+} Imaging and Data Analysis

CRS-based Ca^{2+} imaging in mesophyll protoplasts was employed as previously described[10]. To monitor nitrate-triggered Ca^{2+} changes, the nitrate-free mesophyll protoplasts (2×10^5) in 1 mL buffer were transfected with 100 μg CRS plasmid DNA. The transfected protoplasts were incubated in 5 mL WI buffer for 6 h. Ten millimolar KCl or KNO_3 was added in the buffer solution to stimulate the protoplasts. To monitor ABA-triggered Ca^{2+} changes, 1 mL of 4-week-old mesophyll protoplasts (2×10^5/mL) isolated from soil-grown plants were transfected with 100 μg CRS plasmid. Ten micromolar ABA was added in the solution to stimulate the protoplasts. The images were taken using the Leica AF software on a Leica

DM5000B microscope with the 20× objective lens. The exposure time for GCaMP6s and dTomato was set at 0.5 s and 0.2 s, respectively, and recorded sequentially every 10 s. The fluorescence intensity was determined with the region of interest function for each protoplast. The intensity data were exported and processed using Microsoft Excel software. The images were exported and processed using Adobe Photoshop software.

For Ca^{2+} imaging in the guard and mesophyll cells, root tips, differentiated region of roots, and emerged lateral roots, 10–15 CRS seedlings were grown in one well of a six-well tissue culture plate containing 1 mL of 1/2 MS medium, maintained under 12 h light:12 h dark photoperiod conditions at 23°C for 7 days. To make a chamber slide, two strips of invisible tape were placed onto the long sides of a cover slip (50 mm×24 mm) coated with 45 µL of 1/2 MS medium (described above). The 7-day-old seedlings were embedded in the medium. A thin layer of cotton fiber was placed on top of the cotyledon. A cover slip (24 mm×24 mm) was placed on the sample and secured in place by two strips of invisible tape. The seedling recovered on the slide for 10–20 min. Ca^{2+} imaging was performed using the Leica laser scanning confocal system (Leica TCS SP8X DLS confocal microscope). The stimuli buffer [(15 µL) 1/2 MS medium with 40 µM ABA (A100953, Aladdin) or 0.1% ethanol (mock)] was dispensed along the edge of the cover slip. The final concentration of ABA in the solution was 10 µM. To record the fluorescence images of GCaMP6s and dTomato, excitation was set at 488 nm and 554 nm, respectively, and emission was collected at 497–520 nm and 571–610 nm, respectively. The microscope objective magnification was set at 63×; the scanning resolution for the mesophyll cells, root tips, and elongated region of roots was set at 512×512 pixels, while that for the guard cells and emerged lateral root was 1024×1024 pixels. The images of the mesophyll cells, root tips, and elongated region of roots were captured every 0.868 s, while those of the guard cells and emerged lateral root were captured every 5.12 s. To demonstrate the subcellular localization of different CRS variants in the epidermal cells of the root meristem, the scanning resolution for dTomato was set at 1024×1024 pixels, and dTomato images were captured every 5.12 s. For the Ca^{2+} channel blocker assay, seedlings were pre-treated with 2 mM $GdCl_3$ in 1 mL of 1/2 MS medium or 20 mM EGTA in 1 mL 1/2 MS medium or 50 µM BAPTA in 1 mL Ca^{2+}-free basal medium[10] or 1 mL of 1/2 MS medium (mock) for 30 min. For the root tips, the microscope objective magnification was set at 20×, scanning resolution was set at 1024×1024 pixels, and images were captured every 5.12 s. To determine ABA-induced Ca^{2+} changes in the *pyrpyl112458* and *snrk2.2,2.3,2.6* mutants, the CRS transgenic plants were first crossed with *pyrpyl112458* and *snrk2.2,2.3,2.6*, respectively, and homozygous seeds were obtained through PCR identification. The homozygous seeds were then grown in 1/2 MS medium for 7 days. The images of the root tips were visualized and captured by applying the same specifications mentioned above. To verify that *pyrpyl112458* and *snrk2.2,2.3,2.6* are specific in triggering the calcium signal in response to ABA, the Ca^{2+} changes in the *pyrpyl112458* and *snrk2.2,2.3,2.6* mutants under 10 µM ABA treatment were first recorded; then, after 5 min, 1 mM ATP was added and the recording was continued. To determine NaCl-induced Ca^{2+} changes in the *pyrpyl112458* and *snrk2.2,2.3,2.6* mutants, *pyrpyl112458-CRS* and *snrk2.2,2.3,2.6-CRS* were grown in 1/2 MS medium for 7 days, and then recorded traces of calcium signalling in *pyrpyl112458-CRS* and *snrk2.2,2.3,2.6-CRS* plant root tip cells

stimulated by 200 mM NaCl or H_2O (mock). To detect Ca^{2+} changes triggered by NaCl in the root elongation region, CRS were grown in 1/2 MS medium for 7 days, and then recorded traces of calcium signalling in CRS plant root elongation regions stimulated by 200 mM NaCl or H_2O (mock). The images were visualized and captured by applying the same specifications mentioned above. Images were collected and processed using the Leica Application Suite X, Image J, and Adobe Photoshop software. The trace was produced using the GraphPad Prism software.

The signal values of GCaMP6s and dTomato fluorescence intensity were extracted from the indicated regions. The dynamic fluorescence intensity values ($\triangle F$) were calculated as $(F\text{-}F_0)/F_0$, where F_0 represents the starting point value. In each plot, $\triangle F$ was normalized to the lowest calculated value. The ratio was calculated as $\triangle F_{GCaMP6s} / \triangle F_{dTomato}$. To generate the Ca^{2+} imaging heat map of CRS-PM in the epidermal cell of the primary root meristem, the fluorescence ratio values along the plasma membrane were cropped and calculated. The cropped region was divided into 440 segments. The fluorescence intensity ratio of CRS-PM was calculated and the heat map was generated using the ImageJ and GraphPad Prism softwares, respectively.

GCaMP6s-based Ca^{2+} Imaging and Data Analysis

For Ca^{2+} imaging of the root tip using *GCaMP6s* transgenic seedlings, a chamber slide was made, and two strips of invisible tape were placed along the long sides of a cover slip (50 mm×24 mm) coated with 45 µL of 1/2 MS medium. The 7-day-old seedling was embedded in the medium. A thin layer of cotton fiber was placed on top of the cotyledon. The cover slip (24 mm×24 mm) was placed on the sample and secured in place by two strips of invisible tape. The seedling recovered on the slide for 10–20 min. Ca^{2+} imaging was performed using the Leica laser scanning confocal system (Leica TCS SP8X DLS confocal microscope). The stimuli buffer [(15 µL) 1/2 MS medium with 40 µM ABA (A100953, Aladdin) or 0.1% ethanol (mock)] was dispensed along the edge of the cover slip. The final concentration of ABA in the solution was 10 µM. To record the fluorescence images of GCaMP6s, excitation was set at 488 nm and emission was collected at 497–520 nm. For the root tips, the microscope objective magnification was set at 20×, scanning resolution was set at 512×512 pixels, and the images were captured every 0.868 s. The root tip images were collected and processed using the Leica Application Suite X, Image J, and Adobe Photoshop software. The trace was produced using the GraphPad Prism software. The signal values of GCaMP6s fluorescence intensity were extracted from the indicated regions. The dynamic fluorescence intensity values were calculated as $(F\text{-}F_0)/F_0$, where F_0 represents the starting point value.

Protein expression and in vitro Ca^{2+} binding assay

The plasmid DNA of GCaMP6s or the CRS expression construct was transformed into Rosetta™ 2(DE3) pLysS Competent Cells (MilliporeSigma). The cells were induced by 0.5 mM of IPTG when OD600 nm reached 0.6, and proteins were expressed at 18°C for 18 h. The proteins were purified using Ni-NTA agarose beads (Qiagen), buffer-exchanged into PBS using PD-10 Desalting Columns (GE Healthcare), and concentrated by using Amicon Ultra-0.5 Centrifugal Filter Unit (MilliporeSigma). To determine Ca^{2+}-

dependent fluorescence intensity of CRS, 0.5 μg of purified recombinant protein was diluted in the final volume of 100 μL PBS buffer with or without 10 μM $CaCl_2$ and 1 mM EGTA. The steady-state fluorescence spectra were recorded in Corning® 96 well plates (CLS3925, MilliporeSigma) using a spectramax m5 plate reader (Molecular Devices) at room temperature. The filter set used for GCaMP6s and dTomato are excitation 485 nm/emission 525±15 nm and excitation 545 nm/emission 600 nm, respectively. The fluorescence intensity values were background-subtracted using a buffer control. To analyze the Ca^{2+} binding affinity of CRS and GCaMP6s, 11 Ca^{2+} titrations were generated using a Calcium Calibration Buffer Kit #1 (Molecular Probe, Thermo Fisher Scientific) as described in the manual. The purified protein sample (0.5 μg) was added in the final volume of 100 μL Ca^{2+} titrations. The fluorescence intensity was measured as described above. To calculate the K_d value of CRS, the fluorescence intensity ratio was calculated as GCaMP6s/dTomato and then fit into the Hill equation using GraphPad Prism.

RNA isolation, RT–PCR and RT–qPCR

RNA isolation, RT–PCR, and RT–qPCR were performed as described previously[49]. The primers used for the RT–PCR and RT–qPCR are listed in Table S3 (Supplementary Table 3). The relative gene expression was normalized to the expression of *UBQ10*. The ratio was calculated by comparing the treatment condition to the control condition. Triplicate biological samples were analysed with consistent results.

Imaging and defining the root cap cycle

To observe the root cap morphology changes of the 5-day-old WT and *pyrpyl112458* mutant treated without or with 10 μM ABA at different time points at 3-h invertals, the seedlings were embedded in the ½ MS liquid medium on a slide and then recorded using an ECHO Revolve microscope (ECHO). The microscope objective magnification was set at 10× and the images were captured every 3 h for a total 48 h. Root cap images were collected and processed using the ECHO PRO software (ECHO) and Adobe Photoshop software. After each image capture, each individual seedling was carefully returned from the slide and continued to be treated in a well of a 12-well culture plate with 0.5 mL 1/2 MS liquid medium containing 10 μM ABA or 0.1% ethanol (mock). A root cap cycle was defined from the initial time point (0h) event to the next new same event[40]. To monitor the morphology changes of the complete differentiation program of the root cap in WT and *icpk* seedlings, 5-day-old WT seedlings were pretreated with 0.2 μM 3MBiP for 15 min, and then treated with 10 μM ABA or 0.1% ethanol (mock). Root cap images were captured at 0 h, 24 h, 27 h, 30 h, 33 h, 36 h, 39 h, 42 h, and 45 h time points. For monitoring the root cap morphology changes of WT, *pyrpyl112458* and *snrk2.2,2.3,2.6* seedlings in response to NaCl, 5-day-old seedlings were transferred to 1/2 MS liquid medium containing 50 mM NaCl or H_2O (mock). Root cap cycles were captured at 0 h, 27 h, 30 h, 33 h, 36 h, 39 h, 42 h, 45 h, 48 h, 51 h, 54 h, 57 h, and 60 h time points. The statistical and analytical basis for the root cap cycle was previously described[40]. Bar graphs of the root cap cycle were generated using GraphPad Prism.

Declarations

Acknowledgments

We thank Andrew Diener for critical reading of the manuscript. We thank horticultural plant biology and metabolomics center confocal facility at Fujian Agriculture & Forestry University and life science research core services of Northwest Agriculture & Forestry University for providing confocal microscope service, and Yanqing Wang at NWAFU for confocal microscope technical support. The research is supported by NIH grants (R01GM060493 and R01GM129093) to J.S., and startup fund from NWAFU, NSFC-32370433 and NSFC-32170270 to K.L.

References

1. Cheng, W. H. et al. A unique short-chain dehydrogenase/reductase in Arabidopsis glucose signaling and abscisic acid biosynthesis and functions. Plant Cell. 14, 2723–2743 (2002).
2. Cutler, S. R., Rodriguez, P. L., Finkelstein, R. R., & Abrams, S. R. Abscisic acid: emergence of a core signaling network. Annu Rev Plant Biol. 61, 651–679 (2010).
3. Hauser, F., Li, Z., Waadt, R., & Schroeder, J. I. SnapShot: Abscisic acid signaling. Cell 171, 1708–1708 (2017).
4. Yoshida, T., Revisiting the basal role of ABA – roles outside of stress. Trends Plant Sci. 24, 625–635 (2019).
5. Kuromori, T., Seo, M., & Shinozaki, K. ABA transport and plant water stress responses. Trends Plant Sci. 23, 513–522 (2018).
6. Chen, Q. et al. Phosphorylation of SWEET sucrose transporters regulates plant root:shoot ratio under drought. Nat. Plants. 8, 68–77 (2022).
7. Waadt, R., et al. Plant hormone regulation of abiotic stress responses. Nat Rev Mol Cell Biol. 23, 680–694 (2022).
8. Luan, Sheng, & Wang, C. Calcium signalling mechanisms across kingdoms. Annu Rev Cell Dev Biol. 37, 311–340 (2021).
9. Resentini, F., Ruberti, C., Grenzi, M., Bonza, M.C., & Costa, A. The signatures of organellar calcium. Plant Physiol. 187, 1985–2004 (2021).
10. Liu, K. H. et al. Discovery of nitrate-CPK-NLP signalling in central nutrient-growth networks. Nature 545, 311–316 (2017).
11. Edel, K. H., & Kudla, J. Integration of calcium and ABA signaling. Curr Opin Plant Biol. 33, 83–91 (2016).
12. Albert, R. et al. A new discrete dynamic model of ABA-induced stomatal closure predicts key feedback loops. PLoS Biol. 15, e2003451 (2017).
13. Konrad, K. R., Maierhofer, T., & Hedrich, R. Spatio-temporal aspects of Ca^{2+} signalling: Lessons from guard cells and pollen tubes. J Exp Bot. 69, 4195–4214 (2018).

14. Tan, Y.-Q. et al. Multiple cyclic nucleotide-gated channels function as ABA-activated Ca^{2+} channels required for ABA-induced stomatal closure in Arabidopsis. Plant Cell. 35, 239–259 (2023).
15. Boudsocq, M., & Sheen, J. CDPKs in immune and stress signaling. Trends Plant Sci. 18, 30–40 (2013).
16. Scherzer, S. et al. Multiple calcium-dependent kinases modulate ABA-activated guard cell anion channels. Mol Plant. 5, 1409–1412 (2012).
17. Brandt, B. et al. Calcium specificity signaling mechanisms in abscisic acid signal transduction in Arabidopsis guard cells. eLife 4, e03599 (2015).
18. Liese, A. et al. Imaging of plant calcium-sensor kinase conformation monitors real time calcium-dependent decoding in planta. *Plant Cell.* Koad196 (2023).
19. Sheen J. Ca^{2+}-dependent protein kinases and stress signal transduction in plants. Science 274, 1900–1902 (1996).
20. Choi, H. I. et al. Arabidopsis calcium-dependent protein kinase AtCPK32 interacts with ABF4, a transcriptional regulator of abscisic acid-responsive gene expression, and modulates its activity. Plant Physiol. 139, 1750–1761. (2005).
21. Zhu, S. Y. et al. Two calcium-dependent protein kinases, CPK4 and CPK11, regulate abscisic acid signal transduction in Arabidopsis. Plant Cell. 19, 3019–3036 (2007).
22. Li, Z. et al. Abscisic acid-induced degradation of Arabidopsis guanine nucleotide exchange factor requires calcium-dependent protein kinases. Proc Natl Acad Sci U S A. 115, E4522–E4531 (2018).
23. Allen, G.J. et al., Cameleon calcium indicator reports cytoplasmic calcium dynamics in Arabidopsis guard cells. Plant J. 19, 735–747 (1999).
24. Keinath, N. F. et al. Live cell imaging with r-geco1 sheds light on flg22- and chitin-induced transient $[Ca^{(2+)}]_{cyt}$ patterns in Arabidopsis. Mol Plant. 8, 1188–1200 (2015).
25. Waadt, R., Krebs, M., Kudla, J., & Schumacher, K. Multiparameter imaging of calcium and abscisic acid and high-resolution quantitative calcium measurements using R-GECO1-mTurquoise in Arabidopsis. New Phytol. 216, 303–320 (2017).
26. Waadt, R. et al. Dual-reporting transcriptionally linked genetically encoded fluorescent indicators resolve the spatiotemporal coordination of cytosolic abscisic acid and second messenger dynamics in Arabidopsis. Plant Cell. 32, 2582–2601 (2020).
27. Chen, T. W. et al. Ultrasensitive fluorescent proteins for imaging neuronal activity. Nature 499, 295–300 (2013).
28. Ast, C. et al. Ratiometric Matryoshka biosensors from a nested cassette of green- and orange-emitting fluorescent proteins. Nat commun. 8, 431 (2017).
29. Li, Z., Harper, J.F., Weigand, C., & Hua, J.. Resting cytosol Ca^{2+} level maintained by Ca^{2+} pumps affects environmental responses in Arabidopsis. Plant Phyiol. 191, 2534–2550 (2023).
30. Costa, A., Navazio, L., & Szabo, I. The contribution of organelles to plant intracellular calcium signalling. J Exp Bot. 69, 4175–4193 (2018).

31. Wu, R. et al. The 6xABRE synthetic promoter enables the spatiotemporal analysis of ABA-mediated transcriptional regulation. Plant Physiol. 177, 1650–1665 (2018).
32. Rowe, J. et al., Next-generation ABACUS biosensors reveal cellular ABA dynamics driving root growth at low aerial humidity. Nat. Plants 9, 1103–1115 (2023).
33. Demir, F. et al. Arabidopsis nanodomain-delimited ABA signaling pathway regulates the anion channel SLAH3. Proc Natl Acad Sci U S A. 110, 8296–8301 (2013).
34. Gonzalez-Guzman, M. et al. Arabidopsis PYR/PYL/RCAR receptors play a major role in quantitative regulation of stomatal aperture and transcriptional response to abscisic acid. Plant cell. 24, 2483–2496 (2012).
35. Rodriguez, L. et al. C_2-domain abscisic acid-related proteins mediate the interaction of PYR/PYL/RCAR abscisic acid receptors with the plasma membrane and regulate abscisic acid sensitivity in Arabidopsis. Plant Cell. 26, 4802–4820 (2014).
36. Kumpf, R. P., & Nowack, M. K. The root cap: a short story of life and death. J. Exp. Bot. 66, 5651–5662 (2015).
37. Bennett, T. et al. SOMBRERO, BEARSKIN1, and BEARSKIN2 regulate root cap maturation in Arabidopsis. Plant Cell. 22, 640–654 (2010).
38. Kamiya, M. et al. Control of root cap maturation and cell detachment by BEARSKIN transcription factors in *Arabidopsis*. Development. 143, 4063–4072 (2016).
39. Karve, R., Suárez-Román, F., & Iyer-Pascuzzi, A. S. The transcription factor nin-like protein7 controls border-like cell release. Plant Physiol. 171, 2101–2111 (2016).
40. Shi, C. L. et al. The dynamics of root cap sloughing in Arabidopsis is regulated by peptide signalling. Nat. Plants 4, 596–604 (2018).
41. Boudsocq, M., Droillard, M.-J., Regad, L., & Lauriere, C. Characterization of Arabidopsis calcium-depednent protein kinases: activity or not by calcium. Biochem J. 447, 291–299 (2012).
42. van Zelm, E., Zhang, Y., & Testerink, C. Salt tolerance mechanisms of plants. Annu Rev Plant Biol. 71, 403–433 (2020).
43. Yu, B. et al. Root twisting drives halotropism via stress-induced microtubule reorientation. Dev Cell. 57, 2412–2425 (2022).
44. Zhang, H. et al. ABA promotes quiescence of the quiescent centre and suppresses stem cell differentiation in the Arabidopsis primary root meristem. Plant J. 64, 764–774 (2010).
45. Dubreuil, C., Jin, X., Grönlund, A., & Fischer, U. A local auxin gradient regulates root cap self-renewal and size homeostasis. Curr Biol. 28, 2581–2587 (2018).
46. Liu, K. H. et al. NIN-like protein 7 transcription factor is a plant nitrate sensor. Science 377, 1419–1425 (2022).
47. De Rybel, B. et al. A versatile set of ligation-independent cloning vectors for functional studies in plants. Plant Physiol. 156, 1292–1299 (2011).

48. Zepeda, B., & Verdonk, J. C. RNA extraction from plant tissue with homemade acid guanidinium thiocyanate phenol chloroform (AGPC). Curr Protoc. 2, e351 (2022).
49. Liu, K. H., McCormack, M., & Sheen, J. Targeted parallel sequencing of large genetically-defined genomic regions for identifying mutations in Arabidopsis. Plant methods 8, 12 (2012).

Figures

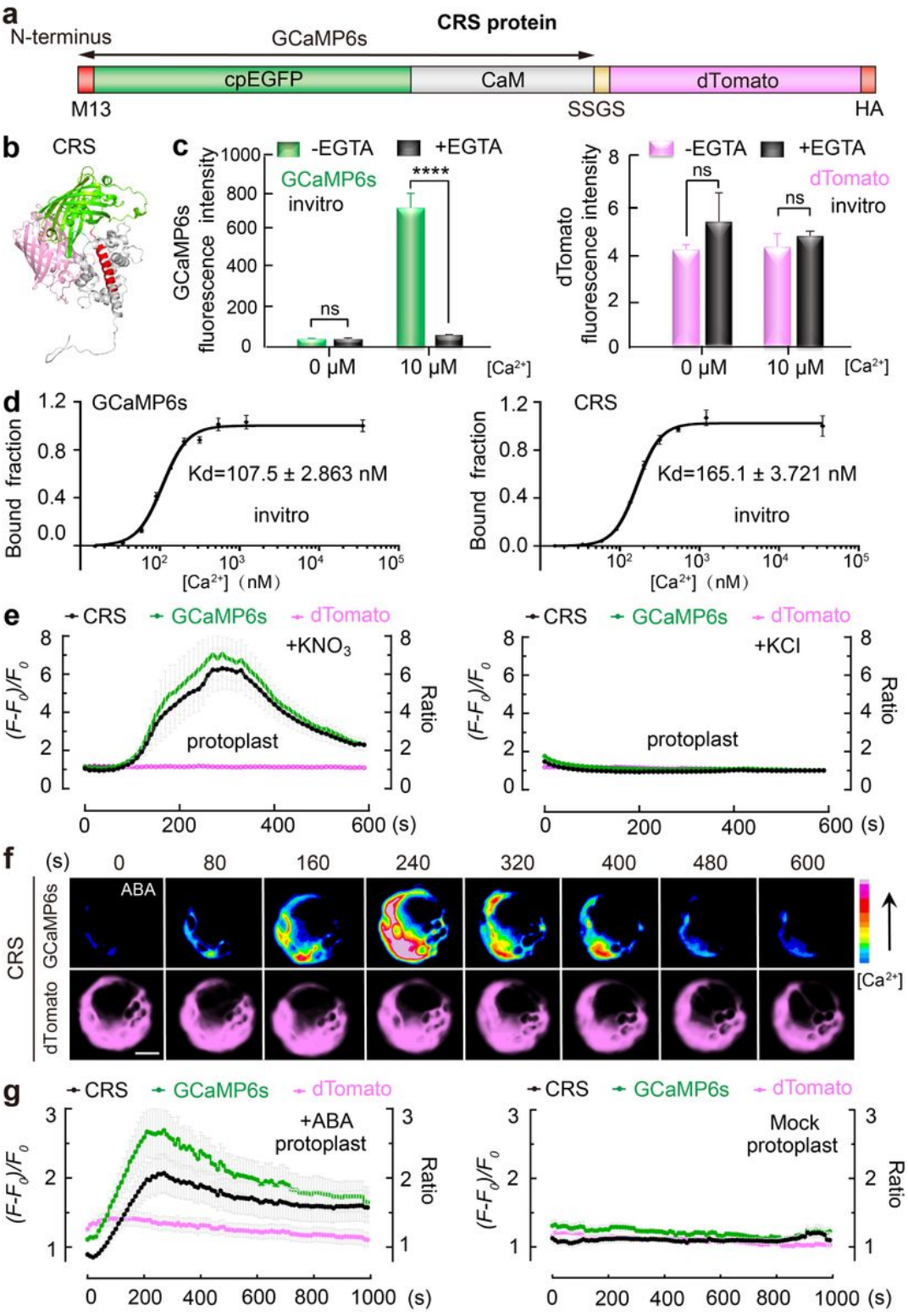

Figure 1

An ultrasensitive Ca^{2+} ratiometric sensor detects ABA-triggered $[Ca^{2+}]$ dynamics.

a, Schemetic presentation of the CRS fusion protein. **b**, Predicted structure of CRS. **c**, CRS protein fluorescence is activated by Ca^{2+} *in vitro*. Green bar, GCaMP6s fluorescence intensity. Pink bar, dTomato fluorescence intensity. Black bar, EGTA. ns P > 0.05, ****P < 0.0001. Error bars denote ±s.e.m., n=3. Statistical significance is determined by two-tailed non-paired Student's *t* test. **d**, Binding affinity of recombinant GCaMP6s and CRS to *in vitro* Ca^{2+}. Error bars denote ±s.e.m., n=3. **e**, Ca^{2+} signatures stimulated by KNO_3 in mesophyll protoplasts expressing CRS. KNO_3, 10 mM. $(F-F_0)/F_0$, relative fluorescence intensity. Ratio, relative fluorescence ratio of GCaMP6s to dTomato. Error bars denote ±s.e.m., n=13 protoplasts. **f**, Time-lapse images of ABA-triggered Ca^{2+} signalling in mesophyll protoplasts expressing CRS. Scale bars, 10 μm. Images are representative of 10 protoplasts. ABA, 10 mM. **g**, CRS signals stimulated by ABA in mesophyll protoplasts expressing CRS. ABA, 10 mM. Scale bars, 10 μm. Error bars denote ±s.e.m., n=13 protoplasts. All experiments were conducted for at least three biological repeats with similar results.

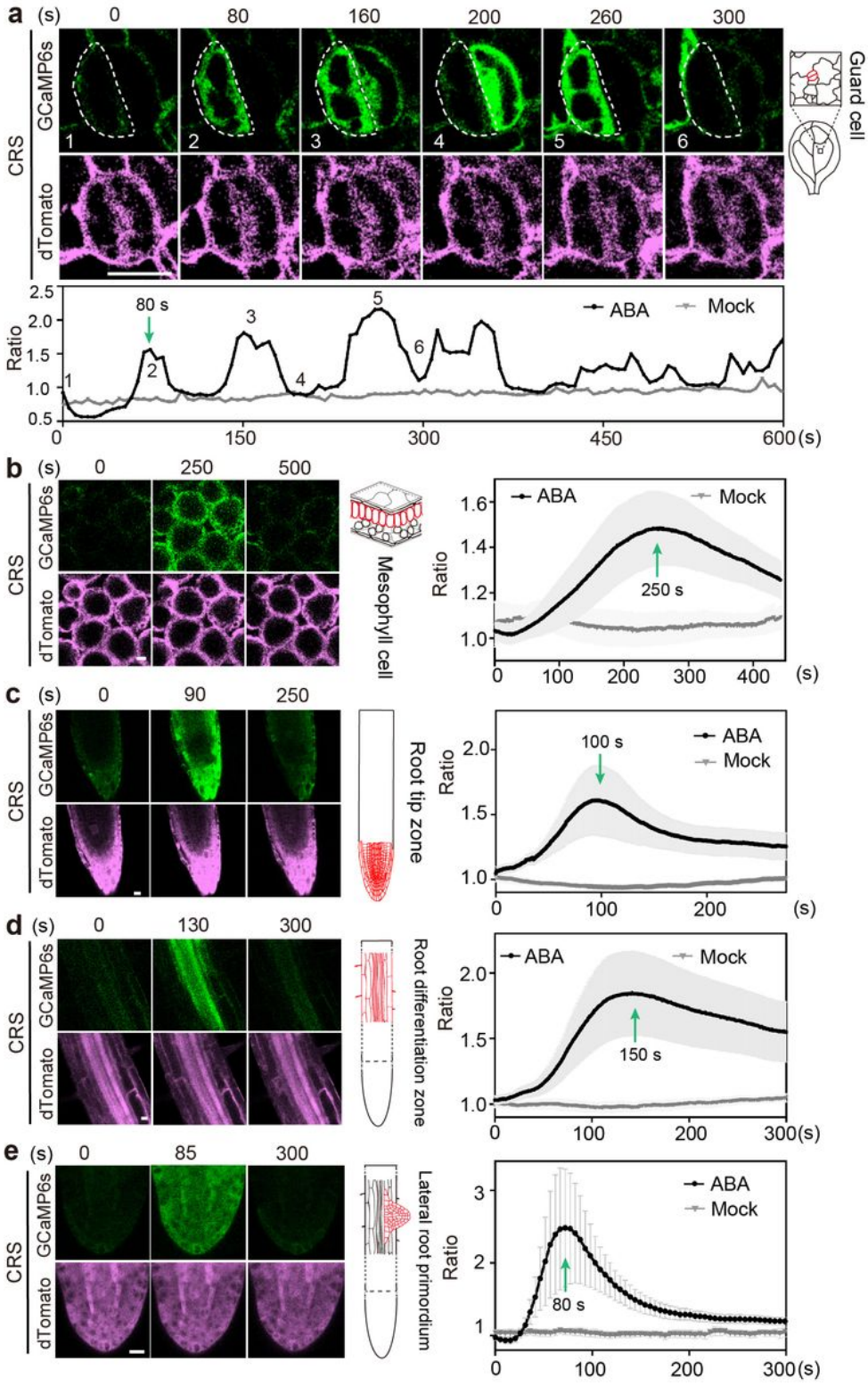

Figure 2

ABA triggers distinct Ca^{2+} signatures in diverse cell types. a-e, Time-lapse images and CRS signals of ABA-stimulated Ca^{2+} signalling. The fluorescence images of GCaMP6s, dTomato, and fluorescence ratio in the guard cells of cotyledons (**a**), mesophyll cells (**b**), root tip (**c**), the root differentiation zone (**d**), and the lateral root primordium (**e**) of 7-day-old transgenic CRS plants. ABA, 10 mM. Green arrows indicate the peak of Ca^{2+} waves. Error bars denote ±s.e.m., n≥6. Scale bars, 10 μm. Ratio, relative fluorescence ratio

of GCaMP6s to dTomato. The monitored region is illustrated in red-lined drawings. All experiments were conducted for at least three biological repeats with similar results.

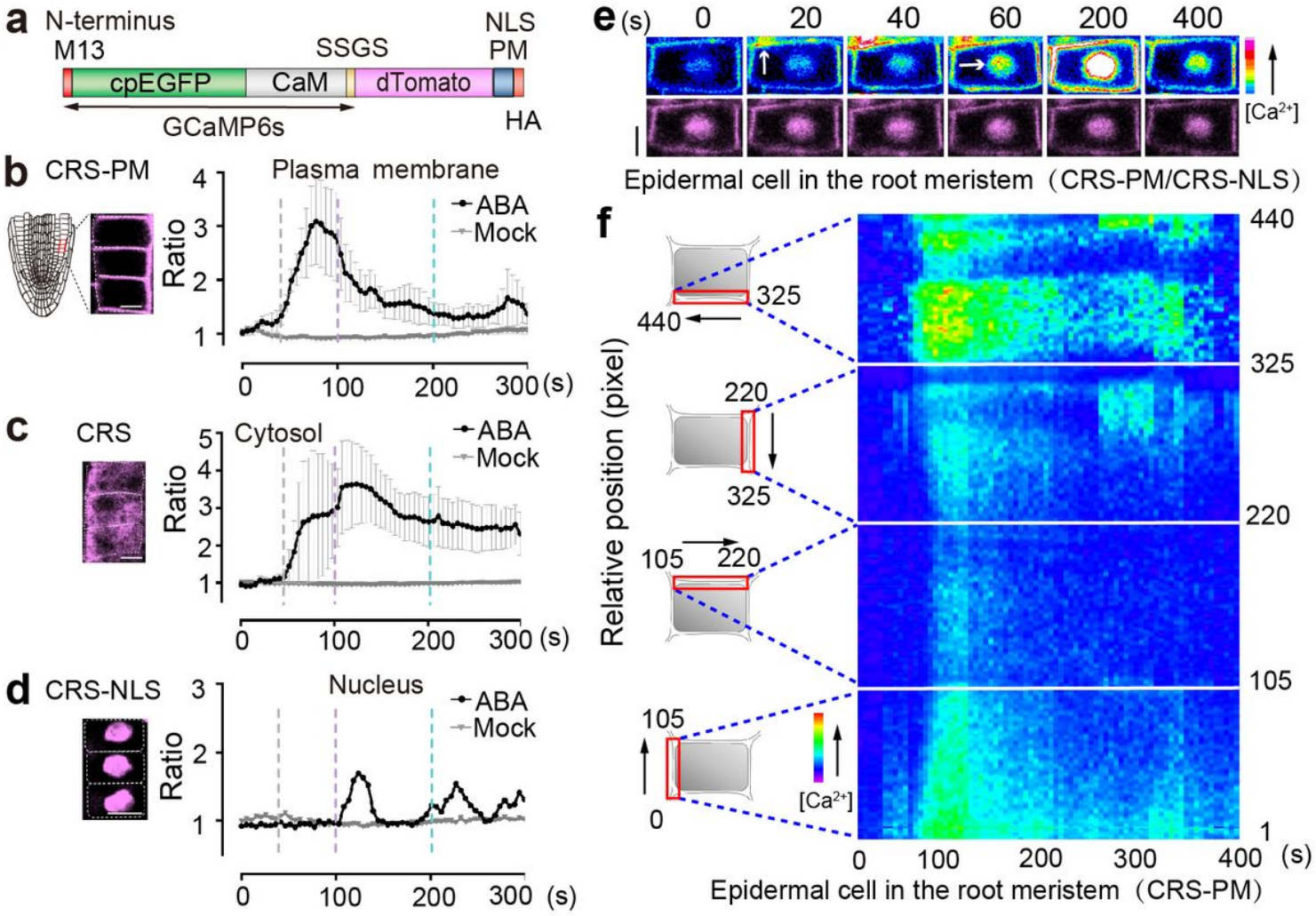

Figure 3

ABA induces spatiotempeoral [Ca^{2+}] dynamics in root cells. a, Schematic presentation of CRS variants targeted to different subcellular compartments. **b-d**, Flurorescence signals of CRS-PM (**b**), CRS (**c**), CRS-NLS (**d**) stimulated by ABA in the epidermal cell of the primary root meristem zone in 7-day-old transgenic plants. ABA, 10 μM ABA. Scale bars, 5 μm. Ratio, relative fluorescence ratio of GCaMP6s to dTomato. Error bars denote ±s.e.m., n=6. The monitored region of the epidermal cell in the root meristem zone is illustrated as red-lined cells. Subcellular localizations of dTomato simages from the CRS derivatives are shown. Gray, purple and green dashed lines indicate 40, 100, and 200 s, respectively, after ABA stimulation. **e**, Time-lapse images of ABA-induced Ca^{2+} wave in the epidermal cell in the root meristem zone of 7-day-old plants expressing both CRS-PM and CRS-NLS. White arrows indicate elevated Ca^{2+} signal. Scale bars, 5 μm. **f**, Kymography analysis of CRS-PM in response to ABA in the root meristem epidermal cell (n=3?). The red lines indicate the region of interest (ROI). The plasma membrane perimeter of a single root epidermal cell was divided into 440 adjacent regions. Images are representative of five

root epidermal cells from three independent experiments. All results were obtained from experiments conducted in at least three biological repeats with similar results.

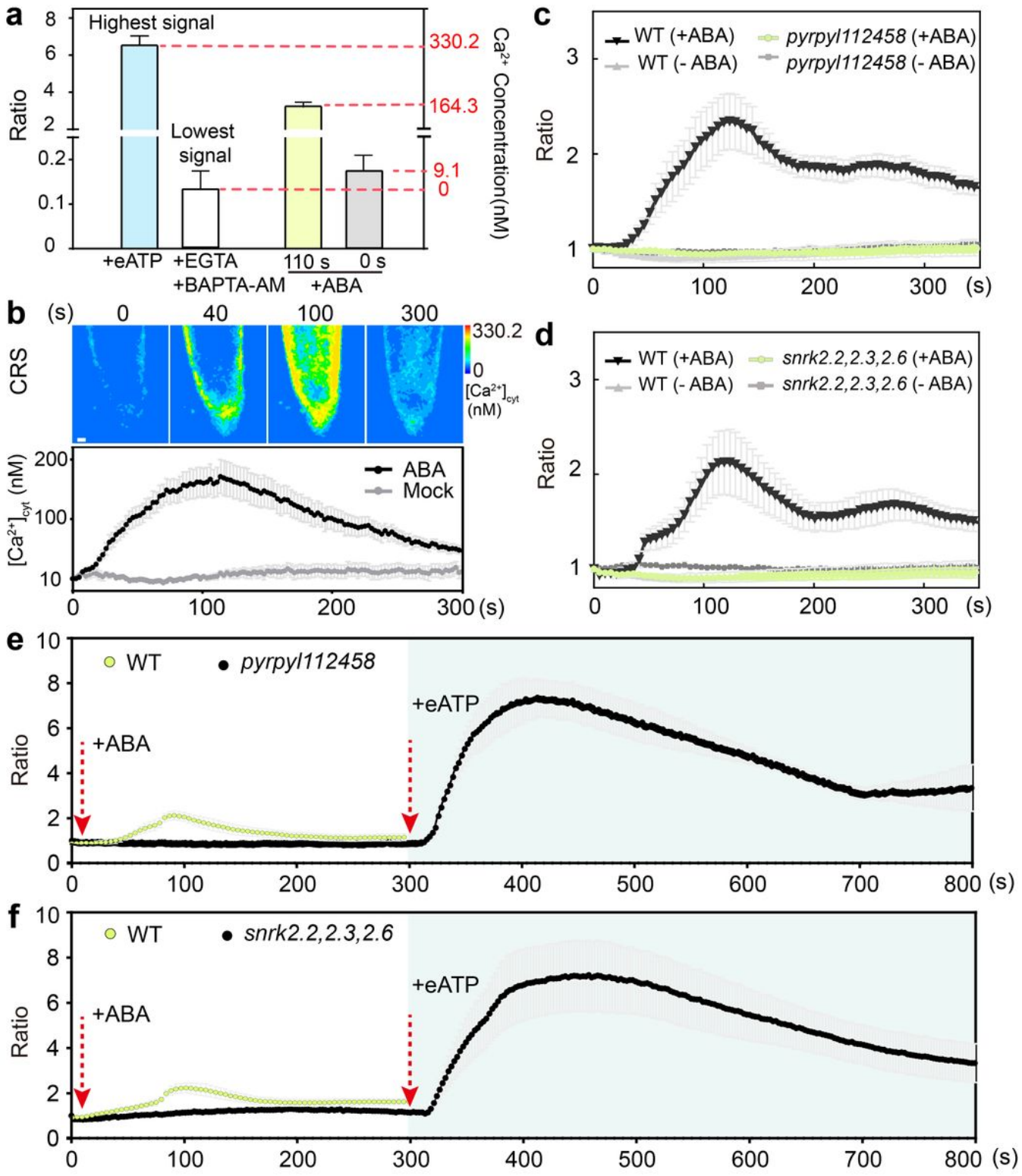

Figure 4

ABA-induced nanomolar [Ca^{2+}] increases via ABA receptor and SNRK2.2/2.3/2.6.

a, Measurement of ABA-induced changes in cytosolic [Ca^{2+}]. The highest [Ca^{2+}] represents eATP-induced [Ca^{2+}] reaching 330.2 nM (blue bar) or the maximum (164.3 nM) stimulated by ABA at the 110 s peak (green bar) in the root tip. The lowest [Ca^{2+}] represents BAPTA-AM and EGTA-treated cells (white bar) or before ABA treatment at 0 s (9.1 nM) (grey bar) in the root tip. Error bars denote ±s.e.m., n=15. Ratio, relative fluorescence ratio of GCaMP6s to dTomato. **b**, Time-lapse images and fluroresence signals of ABA-stimulated [Ca^{2+}] changes in the root tip of 7-day-old transgenic CRS plants. The $[Ca^{2+}]_{cyt}$ denotes cytosolic [Ca^{2+}]. Error bars denote ±s.e.m., n≥10. Scale bars, 10 μm. **c-d**, [Ca^{2+}] waves of the root tip cells stimulated by ABA in 7-day-old WT and *pyrpyl112458-CRS* (**c**) or *snrk2.2,2.3,2.6-CRS* (**d**) plants. Error bars denote ±s.e.m., n=7. **e-f**, [Ca^{2+}] waves in 7-day-old Arabidopsis root tip cells. WT and *pyrpyl112458-CRS* (**e**) or *snrk2.2,2.3,2.6-CRS* (**f**) plant were treated with 10 μM ABA for 5 mins and then with 1 mM eATP. ABA induced [Ca^{2+}] wave (green) in WT but not in the mutants (black) (left panels). Striking [Ca^{2+}] wave was activated by eATP in mutants (black) (right panels). Error bars denote ±s.e.m., n=7. All experiments were conducted in at least three biological repeats with similar results.

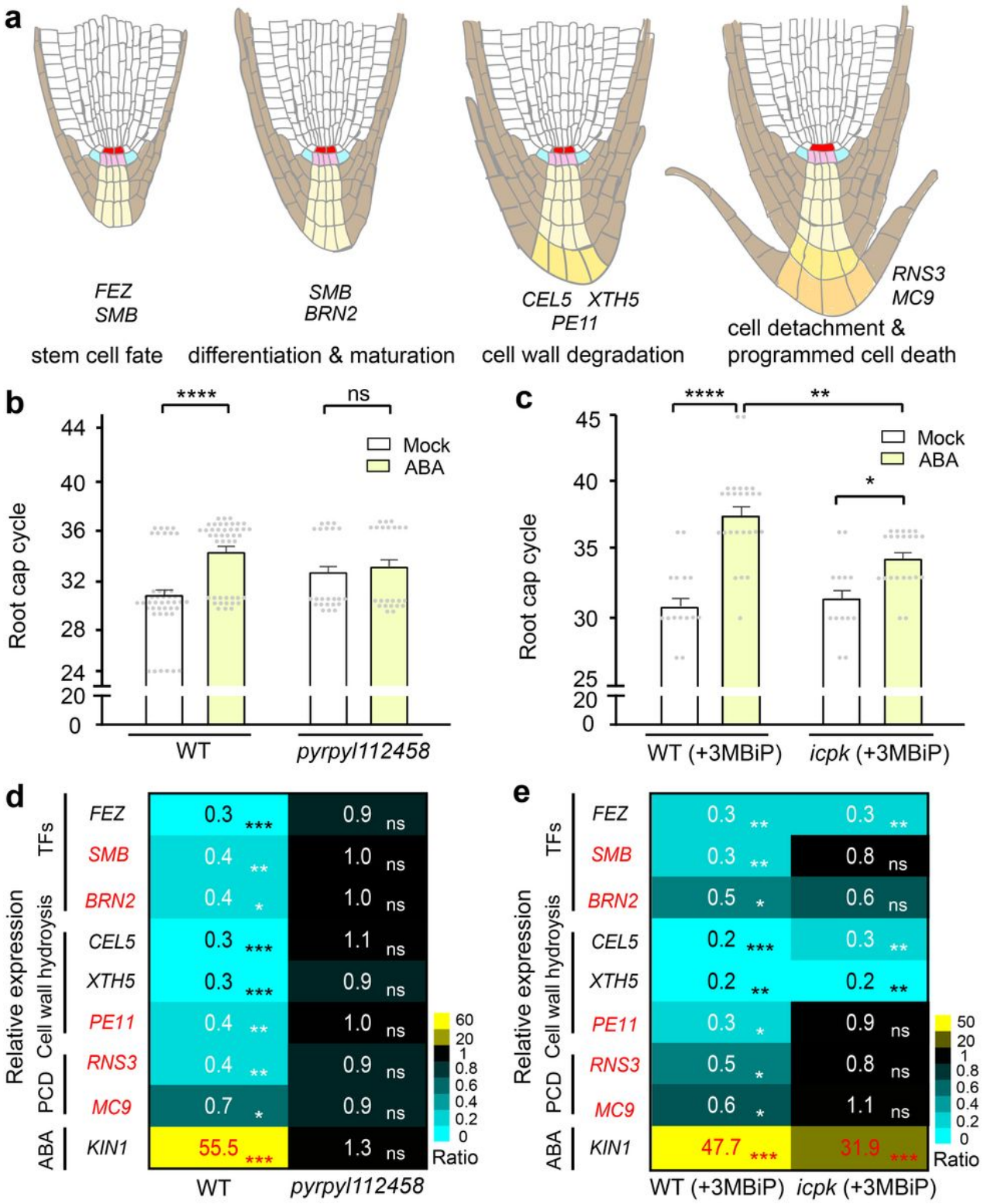

Figure 5

ABA delays the root cap cycle and represses the regulatory gene network. a, The root cap differention program. The multi-step processes include FEZ/SMB regulation of stem cell fate, SMB/BRN2 activation of root cap cell differentiation and maturation, cell wall degradation, and cell detachment and programmed cell death. Red, quiescent center. Pink, columella stem cells. Blue, epidermis/lateral root cap stem cells. Yellow, differentiating and maturing columella cells. Oragne, detached columella cells. Brown,

different stages of lateral root cap cells. **b**, **c**, Delayed root cap cycle in response to ABA treatment. The root cap cycle of 5-day-old WT and *pyrpyl112458* (**b**) or *icpk* (**c**) in root tips was monitored without or with 10 μM ABA treatment. Live imaging of the root cap morphological changes was carried out under a stereo microscope every 3 h for 48 h. Error bars denote ±s.e.m., n≥14. ns (not significant) P > 0.05, ***** P < 0.05, ****** P < 0.01, ******** P < 0.0001. Statistical significance is determined by two-way ANOVA with Tukey's multiple comparisons test. **d**, **e**, Heat map of RT-qPCR analysis of genes central to the root cap differentiation program. Five-day-old WT and *pyrpyl112458* (**d**) or *icpk* (**e**) root tips in response to ABA (10 μM, 4 h) or mock treatment were analyzed. *UBQ10* gene expression was used as a control for normalization. The gene expression level without ABA treatment was valued as 1 in WT or the mutant. The ratio of each marker gene expression was determined. ns (not significant) P > 0.05, ***** P < 0.05, ****** P < 0.01, ******* P < 0.001. Sstatistical significance is determined by multiple unpaired *t*test. TFs, transcription factors. PCD, Programmed cell death. ABA denotes ABA-upregultaed gene. All experiments were conducted in at least three biological repeats with similar results.

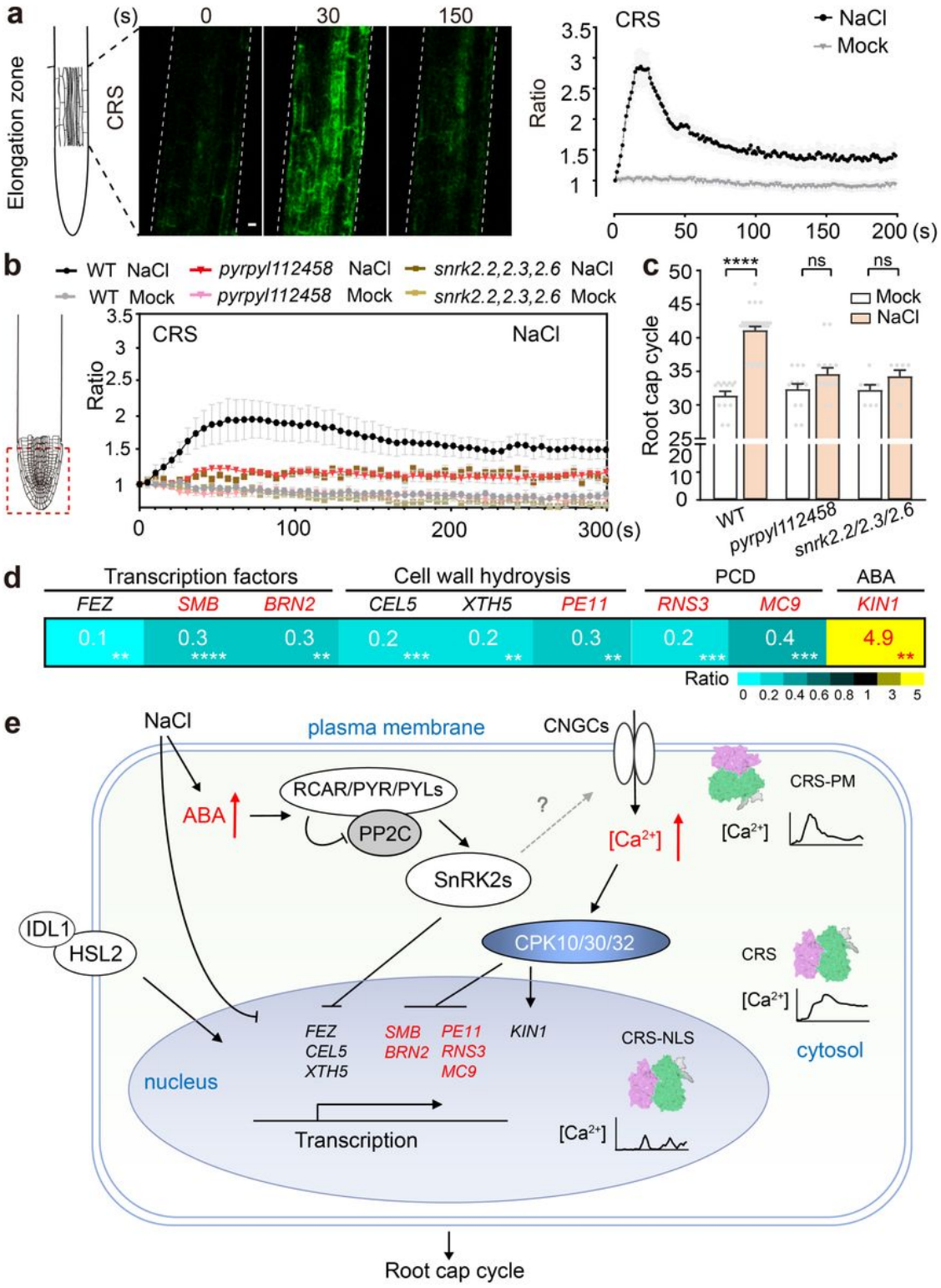

Figure 6

Salt stress triggers a unique [Ca^{2+}] wave in the root tips and delays the root cap cycle. a, Salt stress induces a rapid [Ca^{2+}] spike in the root elongation zone. Time-lapse images and the CRS flurorescence signals of NaCl-stimulated Ca^{2+} signalling in the root elongation zone of 7-day-old plants. NaCl, 200 mM. Error bars denote denote ±s.e.m., n=20. Scale bars, 10 μm. Ratio, relative fluorescence ratio of GCaMP6s

to dTomato. The white dotted line indicates the detection area of the root. **b**, Unique stimulation of [Ca^{2+}] waves by salt. Seven-day-old WT, *pyrpyl112458-CRS* and *snrk2.2,2.3,2.6-CRS* plant root tip cells were stimulated by NaCl. NaCl, 200 mM. Error bars denote ±s.e.m., n=7. **c**, Altered root cap cycle in response to NaCl treatment. Five-day-old WT, *pyrpyl112458 and snrk2.2/2.3/2.6* plants were analyzed. NaCl, 50 mM. Error bars denote ±s.e.m., n≥7. ns (not significant) P > 0.05, **** P < 0.0001. Statistical significance is determined by two-way ANOVA with Tukey's multiple comparisons test. **d**, Heat map of RT-qPCR analysis of genes central to the root cap differentiation program. Five-day-old WT root tip cells in response to 200 mM NaCl or mock treatment were analyzed. ** P < 0.01, *** P < 0.001, **** P < 0.0001. Statistical significance is determined by multiple unpaired *t* test. PCD, Programmed cell death. ABA, ABA-upregulated gene. *UBQ10* gene expression was used as a control for normalization. The gene expression level without salt treatment was valued as 1 in WT. The ratio of each marker gene expression was determined after salt treatment. All experiments were conducted in at least three biological repeats with similar results. **e,** A proposed model for regulating the root cap cycle through Ca^{2+} signaling in response to NaCl stress and ABA treatment. Distinct nanomolar [Ca^{2+}] dynamics triggered by ABA in different subcellular compartments are revealed by CRS-PM, CRS, and CRS-NLS. ABA-triggered [Ca^{2+}] waves act downstream of ABA receptor, RCAR/PYR/PYL and SnRK2s. ABA and Ca^{2+} signaling play crucial roles in regulating genes encoding stem cell TFs and enzymes for cell wall degradation, cell detachment, and programmed cell death in the multiple-step differentiation processes of the root cap cycle. Salt stress induces local ABA elevation and unique [Ca^{2+}] waves in root tip cells, and represses the expression of key root cap cycle genes via CPK10/30/32 signalling.

Supplementary Files

This is a list of supplementary files associated with this preprint. Click to download.

- SupplementaryTable1.pdf
- SupplementaryTable2.pdf
- SupplementaryTable3.pdf
- ExtendedDataFigure1.pdf
- ExtendedDataFigure2.pdf
- ExtendedDataFigure3.pdf
- ExtendedDataFigure4.pdf
- ExtendedDataFigure5.pdf
- ExtendedDataFigure6.pdf
- ExtendedDataFigure7.pdf
- ExtendedDataFigure8.pdf
- ExtendedDataFigurelegends.docx